Appl. Phys. A 69, 471–480 (1999) / Digital Object Identifier (DOI) 10.1007/s003399900156

Applied Physics A
Materials
Science & Processing
© Springer-Verlag 1999

Challenges in predictive calculations of processes at surfaces: surface thermodynamics and catalytic reactions

C. Stampfl[1,*], H.J. Kreuzer[2], S.H. Payne[2], M. Scheffler[1]

[1] Fritz-Haber-Institut der Max-Planck-Gesellschaft, Faradayweg 4-6, D-14195 Berlin-Dahlem, Germany
[2] Department of Physics, Dalhousie University, Halifax, Nova Scotia, B3H 3J5, Canada

Received: 9 May 1999/Accepted: 17 August 1999/Published online: 30 September 1999

Abstract. Obtaining a predictive description of reaction processes at surfaces is one of the goals and challenges of modern theoretical surface science. Over the last few years significant advances have been made in this direction due to increased computer power and methodological developments. In the present paper we describe some recent progress. As a specific example, we discuss our first-principles-based approach for the thermodynamics and kinetics of adparticles at surfaces, which is applied to the system of oxygen at ruthenium. For the same system, we also describe some results of our investigations into the oxidation of CO and the formation of subsurface oxygen species.

PACS: 68.45.Da; 82.65.My; 82.65.Dp

Understanding the complex behavior of atoms and molecules at surfaces requires detailed knowledge of both the macroscopic and microscopic processes that take place. One of the biggest challenges in developing a predictive theory of surface processes is obtaining an accurate description of all associated properties of the system that are relevant on the different space and time scales, and linking them properly. Also other factors such as temperature and gas phase pressure can play a decisive role in the behavior of the system so that it is also desirable to take them into account; furthermore, often interesting phenomena occur far away from thermal equilibrium so that in order to understand such processes, additional theoretical descriptions are required that go beyond ground-state and equilibrium properties. For example, for some systems, the behavior under ultrahigh vacuum (UHV) conditions and "low" temperature (for example, room temperature and below) may be separated from, and different to, the behavior at high gas phase pressures and temperatures by the so-called pressure gap. Thus, although there exists a number of examples for which extrapolation of data over a wide pressure range has been demonstrated to be justified [1], conclusions based on UHV results may not necessarily, or in general, be relevant or valid at high pressures and temperatures. Such a scenario is schematically illustrated in Fig. 1. Under UHV conditions and low temperatures it may be that only a low coverage of ordered or disordered adsorbates is attainable on the surface (i.e., the apparent saturation coverage); at elevated temperatures and pressures there will be a gas phase pressure of particles in contact with the surface and there may be a higher coverage on the surface and even occupation of subsurface sites may occur, due to the additional (thermal) energy available and the higher attempt frequencies to overcome kinetic barriers and barriers for diffusion into the surface.

In the literature, several studies have been reported over recent years that represent notable progress in approaches aimed at providing a predictive description of processes at surfaces, for example, the dynamics of dissociative adsorption of diatomic molecules. This appears to be one of the simplest of surface reactions, yet its accurate theoretical description is actually very involved. Earlier studies of such reactions were based largely on semi-empirical potential energy surfaces (PESs), i.e., the total energy as a function of the atomic coordinates. Such energy surfaces describe the atoms' dynamics, for example vibrations, rotations, center-of-mass translation, scattering from the surface, dissociation, and diffusion. These PESs were restricted in their dimensionality in that only a small number of the reaction coordinates

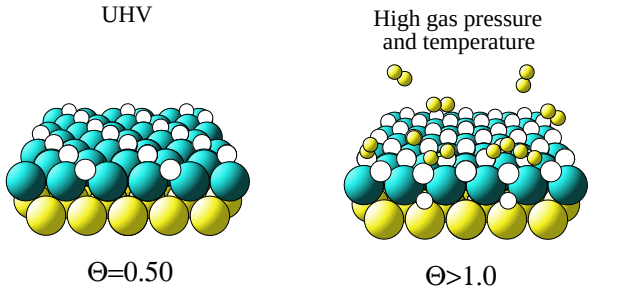

Fig. 1. Schematic illustration of possible adsorbate arrangements for low (gas phase) pressure and temperature (*left panel*) and for high (gas phase) pressure and elevated temperature (*right panel*)

* Corresponding author.
(Fax.: +1-847/491-5082, E-mail: cathy@venus.phys.nwu.edu)

were considered (e.g. the distance between the atoms of the dissociating molecule and their perpendicular distance from the surface), whereas in reality there are at least six important coordinates (for example the x, y, z coordinates of the two atoms – assuming the surface remains rigid throughout the dissociation process, which we note may not always be a valid assumption). The dynamics of atoms can be treated classically, i.e. by Newton's equations of motion, using the forces acting on the atoms as determined from the underlying PES, or they can be treated quantum mechanically. More recent studies, so far mainly applied for hydrogen at surfaces, have been performed using ab initio PESs which have also taken into account the high dimensionality of the system as well as extensive statistics. These calculations (see for example [2–4] and references therein) demonstrated the importance of such an accurate description for the understanding of certain behavior. For the ab initio PES for H_2 dissociation, it has been found that the generalized gradient approximation (GGA) for the exchange-correlation function represents a significant improvement in obtaining activation energies consistent with experiment; the local density approximation (LDA) severely underestimates the energy barriers [5, 6]. One may also expect the GGA to yield an improved description for other reactions at surfaces involving bonds that are being broken and reformed. Consideration of the high dimensionality of the PES is clearly necessary since particles will be incident at a surface in many possible orientations and directions and the energetics of the system can differ dramatically depending on their coordinates (for example some pathways may be non-activated (no energy barrier) while others may be activated). Owing to the demanding nature of obtaining ab initio PESs, the calculated points may be interpolated using analytic or numerical representations, and for trajectory calculations this is required [2, 3]. Furthermore, a good treatment of the statistics of the many possible trajectories has been found to be extremely important, since ultimately the statistical average over many trajectories determines the final result, for example probability of dissociation (sticking) or reflection. Other important factors determining the outcome are the incident energy and rotational and vibrational states of the particle; the latter two properties can only be treated in a quantum description [2]. In fact, for understanding certain phenomena it may be necessary to treat light atoms such as hydrogen as quantum particles.

Complicating factors with respect to obtaining a realistic and predictive description of surface processes, in general, are (i) electronic excitations. These are outside the Born–Oppenheimer approximation [7], which decouples the dynamics of the electrons and nuclei so that whatever the motion of the nuclei, the electrons are in the ground state of the instantaneous geometry; and (ii) the dynamics of the substrate may be important, in particular, for reactions involving heavier and more reactive species than hydrogen, as well as effects of temperature and gas phase partial pressures.

Another area where predictive first-principles-based simulations of surface processes have been applied is in the area of crystal growth and surface diffusion, in particular, kinetic Monte Carlo calculations have been performed with parameters (for example diffusion barriers, place-exchange energies, attachment energies, etc.) derived from first-principles calculations, for metals [8] and semiconductor surfaces [9]. These studies include long time scales (for example seconds) and describe meso- and macroscopic dimensions permitting a detailed comparison with experiment (for example, scanning tunneling microscopy (STM)). For these involved simulations, it is not always clear a priori whether all important microscopic processes have been included; additional ones, however, can be added to provide a more accurate description which, in any case, may add to the understanding of the relevance of the various microscopic mechanisms. Also equilibrium shapes of quantum dots on surfaces have been investigated using a combination of ab initio calculations and macroscopic theories [10]. Here, microscopic parameters such as surface (and edge) energies and surface stresses are coupled with elasticity theory for describing the long-range strain fields and strain relaxations. We would also like to mention that bulk alloy systems have been extensively studied through the combination of first-principles calculations and appropriate statistical mechanical descriptions [11].

In the following we describe our first-principles-based approach for surface thermodynamics and kinetics of adparticles at surfaces. In this theory we link physical properties of microscopic processes with those on the macroscopic scale, including temperature and (gas phase) pressure in the description. Briefly, we use the microscopic energies provided by density functional theory (DFT), the statistical mechanical approach of a lattice gas model for which we evaluate the partition function using transfer matrix techniques [12], and analytic rate equations employing the calculated temperature- and coverage-dependent adsorbate chemical potential. By way of example, we study oxygen at the Ru(0001) surface for which detailed structural [13–18], kinetic [19], and thermodynamic [20, 21] experimental data are available. We also describe results of our study of the heterogeneous catalytic reaction of carbon monoxide oxidation over the O-covered ruthenium surface, as well as the formation of subsurface oxygen species. The presence of highly mobile subsurface oxygen species have been identified to exist in a specific temperature and (O_2) pressure window and have been attributed to giving rise to CO_2 formation rates orders of magnitude higher than previously reported for this system.

1 Surface thermodynamics and kinetics

To describe the kinetics of adsorption, desorption, surface diffusion, and surface reactions one can apply macroscopic kinetic rate equations which are functions of macroscopic variables, for example (local) coverage, partial pressures, temperature. This approach requires that the adsorbate is in local thermodynamic equilibrium. A more general treatment that does not have this restriction is provided by the kinetic lattice gas model. Typically it is not a truly microscopic description since it is based on a phenomenological hamiltonian. For a more accurate and predictive description, and greater understanding of the physical processes, it is necessary to start from a *microscopic* Hamiltonian. In the present work, which we recently reported in [22], this is what we have done through the use of ab initio calculations to construct a lattice gas Hamiltonian. It is written as:

$$
\begin{aligned}
H = & E_s^{\mathrm{hcp}} \sum_i n_i + E_s^{\mathrm{fcc}} \sum_i n_i + 1/2 \Bigg(V_{1\mathrm{n}}^{\mathrm{hcp}} \sum_{i,a} n_i n_{i+a} \\
& + V_{1\mathrm{n}}^{\mathrm{fcc}} \sum_{i,a} n_i n_{i+a} + V_{1\mathrm{n}}^{\text{hcp-fcc}} \sum_{i,a'} n_i n_{i+a'} \\
& + V_{2\mathrm{n}}^{\mathrm{hcp}} \sum_{i,b} n_i n_{i+b} + V_{2\mathrm{n}}^{\mathrm{fcc}} \sum_{i,b} n_i n_{i+b} \\
& + V_{2\mathrm{n}}^{\text{hcp-fcc}} \sum_{i,b'} n_i n_{i+b'} + V_{3\mathrm{n}}^{\mathrm{hcp}} \sum_{i,c} n_i n_{i+c} \\
& + V_{3\mathrm{n}}^{\mathrm{fcc}} \sum_{i,c} n_i n_{i+c} + V_{3\mathrm{n}}^{\text{hcp-fcc}} \sum_{i,c'} n_i n_{i+c'} \\
& + V_{\mathrm{trio}}^{\mathrm{hcp}} \sum_{i,a,a''} n_i n_{i+a} n_{i+a''} \\
& + V_{\mathrm{trio}}^{\mathrm{fcc}} \sum_{i,a,a''} n_i n_{i+a} n_{i+a''} + \ldots \Bigg), \qquad (1)
\end{aligned}
$$

where the index i distinguishes surface unit cells, the occupation numbers n_i are 0 or 1 depending on whether a site in cell i is empty or occupied and sumations are also over neighboring sites. Equation 1 incorporates interactions between atoms in hcp sites, or in fcc sites, as well as interactions between atoms in hcp and fcc sites (as indicated by the label "hcp-fcc"). The indicies a, b, and c indicate the first, second, and third-neighbor distances between atoms in like sites, while indices a', b', and c' represent those between atoms in fcc and hcp sites (unlike sites). Here $E_s^{\mathrm{hcp}} = -V_a - k_{\mathrm{B}} T \ln q_3$ is the free energy of an isolated O atom in an hcp site with V_a being the (positive) depth of the adsorption potential, referenced to an atom at rest in the gas phase over the surface. Relative to a molecule in the gas phase, which dissociates at the surface, we can define the electronic binding energy of an atom as $V_0 = -(V_a - 1/2 E_{\mathrm{diss}})$, with E_{diss} the electronic component of the gas phase molecule dissociation energy. q_3 is the atom partition function accounting for its motion on the surface: $q_3 = q_z q_{xy}$; $q_z = \exp(h\nu_z/2k_{\mathrm{B}}T) / \left[\exp(h\nu_z/k_{\mathrm{B}}T) - 1\right]$ is the component for vibration perpendicular to the surface; likewise, q_{xy} is the partition function for frustrated translation parallel to the surface. $V_{1\mathrm{n}}^{\mathrm{hcp}}$, $V_{2\mathrm{n}}^{\mathrm{hcp}}$, and $V_{3\mathrm{n}}^{\mathrm{hcp}}$ are the first, second, and third-neighbor (two-body) interaction energies between O atoms in hcp sites, with analogous definitions for terms labeled "fcc" and "hcp-fcc". Trio interaction energies, V_{trio}, account for additional modifications due to the change in the interaction between two adsorbed O atoms when a third adatom is adsorbed close by; three types of trio interactions are taken into account (see below). For further details we refer to [23, 24].

As noted above, we perform electronic structure calculations using DFT in order to obtain the PES of adparticles on the surface for different coverages, $\theta = \langle n_i \rangle$, and geometries. The actual structures calculated are shown in Fig. 2. The DFT calculations are performed using the pseudopotential [25, 26] plane wave method [27] with the GGA [28] for the exchange-correlation function. The surface is modeled using the supercell approach with four atomic layers of Ru and the O atoms adsorbed on one side. We fully relax the positions of the O atoms and the top two Ru layers. Further technical details can be found in [29].

The adsorption energy per adatom is defined as

$$
E_a = 1/n \left[E_{\mathrm{total}}^{\mathrm{O/Ru}} - E_{\mathrm{total}}^{\mathrm{Ru}} - n \left(1/2 E_{\mathrm{total}}^{\mathrm{O_2}} \right) \right], \qquad (2)
$$

where $E_{\mathrm{total}}^{\mathrm{O/Ru}}$, $E_{\mathrm{total}}^{\mathrm{Ru}}$, and $E_{\mathrm{total}}^{\mathrm{O_2}}$ are the total energies of the O/Ru(0001) adsorbate system, the clean Ru surface (as calculated using exactly the same supercells), and a free O_2 molecule, respectively; n is the number of O atoms in the surface unit cell. The energy of a free O_2 molecule is calculated relative to that of two free O atoms and yields an electronic energy difference of $E_{\mathrm{diss}} = 5.95$ eV. This value is larger than experiment (≈ 5.2 eV) but is typical of present-day DFT-GGA calculations for O_2. We note that typically, although DFT-GGA calculated adsorption energies reduce the overbinding of the local-density approximation (LDA), there is still a slight overbinding so that with $1/2O_2$ as the reference, we obtain some cancellation of errors. We have performed calculations for O in both the hcp and fcc sites as well as for structures involving both hcp and fcc site occupation (see Fig. 2). Since ruthenium is of hexagonal close-packed crystal structure, the "hcp site" for the O atom has a Ru atom directly below it in the second substrate layer and the "fcc

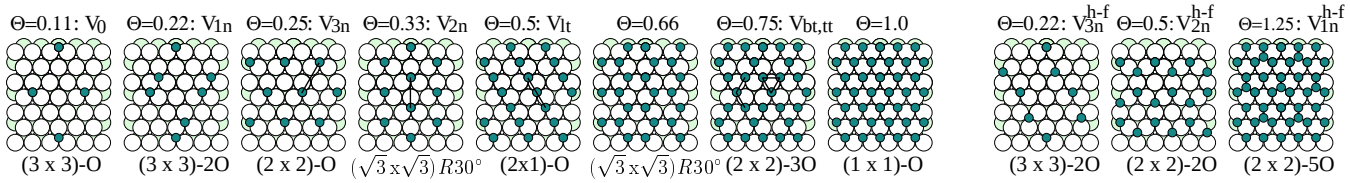

Fig. 2. Adsorbate structures calculated using DFT-GGA. For the first eight diagrams analogous calculations were also performed for O in fcc sites. Small circles represent O atoms and large circles, Ru atoms

Table 1. Average adsorption energies per atom (in eV) for O on Ru(0001) with respect to $1/2O_2$ for various coverages and structures

Site	$V_0 = E_a^{\theta=1/9}$	$E_a^{\theta=2/9}$	$E_a^{\theta=1/4}$	$E_a^{\theta=1/3}$	$E_a^{\theta=1/2}$	$E_a^{\theta=2/3}$	$E_a^{\theta=3/4}$	$E_a^{\theta=1}$	Site	$E_{a,\mathrm{hcp-fcc}}^{\theta=2/9}$	$E_{a,\mathrm{hcp-fcc}}^{\theta=1/2}$	$E_{a,\mathrm{hcp-fcc}}^{\theta=5/4}$
hcp	−2.503	−2.417	−2.577	−2.370	−2.307	−2.150	−2.091	−1.895	hcp−fcc	−2.294	−2.209	−1.492
fcc	−2.152	−2.107	−2.145	−2.105	−2.025	−2.015	−1.942	−1.865				

site" does not. The obtained adsorption energies are listed in Table 1.

In order to determine the interaction parameters in (1), we express the adsorption energies (for both hcp and fcc sites) as,

$$
\begin{aligned}
E_a^{\theta=2/9} &= V_0 + \frac{1}{2}(V_{1\mathrm{n}} + V_{3\mathrm{n}}) \quad , \\
E_a^{\theta=1/4} &= V_0 + 3V_{3\mathrm{n}} \, , \\
E_a^{\theta=1/3} &= V_0 + 3V_{2\mathrm{n}} \quad , \\
E_a^{\theta=1/2} &= V_0 + V_{1\mathrm{n}} + V_{2\mathrm{n}} + 3V_{3\mathrm{n}} + V_{\mathrm{lt}} \quad , \\
E_a^{\theta=2/3} &= V_0 + \frac{3}{2}V_{1\mathrm{n}} + 3V_{2\mathrm{n}} + \frac{3}{2}V_{3\mathrm{n}} + 3V_{\mathrm{bt}} \quad , \\
E_a^{\theta=3/4} &= V_0 + 2V_{1\mathrm{n}} + 2V_{2\mathrm{n}} + 3V_{3\mathrm{n}} + 2V_{\mathrm{lt}} + 2V_{\mathrm{bt}} + \frac{2}{3}V_{\mathrm{tt}} \quad , \\
E_a^{\theta=1.0} &= V_0 + 3(V_{1\mathrm{n}} + V_{2\mathrm{n}} + V_{3\mathrm{n}}) + 3V_{\mathrm{lt}} + 6V_{\mathrm{bt}} + 2V_{\mathrm{tt}} \quad .
\end{aligned}
$$

V_{lt}, V_{bt}, and V_{tt} are linear, bent, and triangular trios where the three nearest-neighbor O atoms form a line, a kink, and a triangle, respectively (as indicated in Fig. 2). The adsorption energy for an isolated O atom, V_0, is taken to be that of O in the (3×3) structure. With this large O−O separation, which corresponds to the fifth-neighbor distance, the interaction is negligible. We note that for the (3×3)-2O structure at $\theta = 2/9$ where there are two O atoms in nearest-neighbor sites, on allowing lateral relaxations, the O atoms move significantly from the locally three-fold symmetric adsorption sites to reduce the strong repulsion, $V_{1\mathrm{n}}$. With such strong nearest neighbor repulsion, isolated nearest neighbor pairs are in fact highly improbable. We therefore calculated $E_a^{\theta=2/9}$ for atoms at locally three-fold symmetric sites because if we were to use the energetics of the laterally relaxed structure, we would have to include yet higher many-body interactions (i.e., longer-ranged trios, quartos, and quintos, etc.) to account for the movement of the atoms *back* to the ideal three-fold sites which occurs for higher coverages. Thus, we observe that, even in our elaborate description, the microscopic Hamiltonian is not yet quite complete.

Using the first six of the seven equations above, we obtain the interaction energies listed in Table 2. Using these parameters to evaluate the energy of the monolayer coverage as given by the seventh equation, we find a value of 0.034 eV smaller than that of the DFT-GGA value. Alternatively, using the seventh equation to obtain the interaction parameters and the sixth one as a cross-check, the obtained energy differs by only 0.011 eV (less) compared to the self-consistently calculated DFT-GGA result. This gives us a gauge of the accuracy. We also derived interaction parameters for interactions between O atoms occupying neighboring hcp and fcc sites which were obtained from the last three diagrams of Fig. 2 by writing down appropriate equations in an analogous manner to those listed above, i.e.,

$$
\begin{aligned}
E_a^{\theta=2/9} &= [V_0^{\mathrm{hcp}} + V_0^{\mathrm{fcc}} + V_{3\mathrm{n}}^{\mathrm{hcp-fcc}}]/2 \, , \\
E_a^{\theta=1/2} &= [E_a^{\theta=1/2,\mathrm{hcp}} + E_a^{\theta=1/2,\mathrm{fcc}} + 3V_{3\mathrm{n}}^{\mathrm{hcp-fcc}}]/2 \, , \\
E_a^{\theta=5/4} &= [E_a^{\theta=1,\mathrm{hcp}} + E_a^{\theta=1/4,\mathrm{fcc}} + 3V_{1\mathrm{n}}^{\mathrm{hcp-fcc}} + 3V_{2\mathrm{n}}^{\mathrm{hcp-fcc}} \\
&\quad + 6V_{3\mathrm{n}}^{\mathrm{hcp-fcc}}]/5 \, .
\end{aligned}
$$

In Table 2 we give in brackets the interactions energies determined by Piercy et al. [19]. It can be seen that, in general, the magnitudes and signs are close to those determined by DFT-GGA, but that there are some differences, for example for $V_{1\mathrm{n}}^{\mathrm{fcc}}$, by more than 50%. In fact we expect some deviations since the parameters of [19] are only obtained by adjustment to fit experimental data, and may not necessarily therefore be unique or transferable. The calculated values of $V_{2\mathrm{n}}$ and $V_{3\mathrm{n}}$ may be compared to pairwise interactions between O atoms of 26–30 meV and −45 to −50 meV), respectively as obtained from STM experiments [30].

In [19], in order to obtain a satisfactory explanation of the surface phase diagram in the vicinity of the order−disorder transition temperature, it was found that a spillover into fcc sites of about 12% occurs. From Table 2, it can be seen that for low coverage the hcp site is significantly more favorable than the fcc site, and that with increasing coverage the adsorption energies decrease, as does the energy difference between the hcp and fcc sites, but that the hcp site is always energetically favorable. Thus a spillover effect could be plausible at least at the higher coverages. In relation to this we considered the energy barrier for diffusion from the hcp site to the fcc site via the bridge site for coverage 1/4 as obtained by laterally shifting the (2×2) overlayer. We find a barrier of 0.69 eV (see lower curve of Fig. 3) which is in very good agreement with the value of 0.7 eV as determined by STM experiments [31]. Given that at this coverage the fcc site is about 0.43 eV less favorable that the hcp site, and that the barrier for the reverse diffusion path, i.e. from the fcc site into the hcp site (via the bridge site) is only 0.26 eV (see Fig. 3), it is expected that occupation of fcc sites will actually be very short lived at el-

Table 2. DFT-GGA calculated interaction energies (in eV) for O on Ru(0001). In parenthesis are the interaction parameters used by Piercy et al. [19]

Site	$V_{1\mathrm{n}}$	$V_{2\mathrm{n}}$	$V_{3\mathrm{n}}$	V_{lt}	V_{bt}	V_{tt}
hcp	0.265 (0.23)	0.044 (0.069)	−0.025 (−0.023)	−0.039	−0.046	0.058
fcc	0.158 (0.069)	0.016	0.002	−0.052	−0.044	0.076
fcc−hcp	0.586	0.101	0.033			

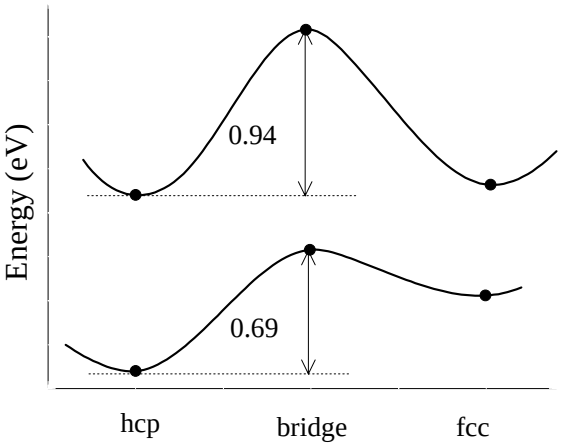

Fig. 3. Schematic illustration of the diffusion path for O going from the hcp to the fcc site via the bridge site for an O coverage of 0.25 (*lower curve*) and 1.0 (*upper curve*) monolayers

evated temperatures and thus will not play an important role at lower coverages. For one monolayer coverage the analogous diffusion barrier is found to be 0.94 eV (see upper curve of Fig. 3).

Finally, construction of our Hamiltonian also requires vibrational frequencies which are calculated using DFT; for example, we obtain for the vibration of oxygen normal to the surface (at the $\overline{\Gamma}$-point) $\nu_z = 509\,\mathrm{cm}^{-1}$ and for the free O_2 molecule, $1519\,\mathrm{cm}^{-1}$. The experimental values are $535\,\mathrm{cm}^{-1}$ [32] (for O in the (2×2) phase) and $1580\,\mathrm{cm}^{-1}$ [33], respectively.

Having determined the Hamiltonian, transfer matrix techniques, which allow a straightforward evaluation of the adsorbate partition function, are used to determine thermodynamic information about the system, for example, the chemical potential as a function of coverage and temperature. We note that the transfer matrix method [34] has also been used to determine phase diagrams and critical-point properties of adsorbates [35, 36] and magnetic spin systems [37, 38]. With respect to its more recent application, as in the present work, to desorption rates and heats of adsorption (described below), we refer to a very recent review for details [12].

The kinetic equation for adsorption and desorption is written as $\mathrm{d}\theta/\mathrm{dt} = R_{\mathrm{ad}} - R_{\mathrm{des}}$, where, for an atomic adsorbate in contact with a gas of diatomic homonuclear molecules, the rate of adsorption is $R_{\mathrm{ad}} = 2\mathrm{S}_{\mathrm{dis}}(\theta, T)P_m a_{\mathrm{s}}\lambda_m/h$. P_m is the molecular pressure above the surface, a_{s} is the area of one surface unit cell, $\lambda_m = h/(2\pi m k_{\mathrm{B}}\mathrm{T}^{1/2}$ is the thermal wavelength of a molecule of mass m, and $S_{\mathrm{dis}}(\theta, T)$ is the dissociative sticking coefficient. Under the assumption that the adsorbate remains in quasi-equilibrium during the desorption process i.e., this process has the slowest time scale of all processes occurring at the surface, the desorption rate can be factored into a dynamic part, i.e., the sticking coefficient, and a thermodynamic part involving the fugacity and is given by [23],

$$R_{\mathrm{des}} = 2\mathrm{S}_{\mathrm{dis}}(\theta, T)a_{\mathrm{s}}\frac{k_{\mathrm{B}}T}{h\lambda_m^2}\frac{Z_{\mathrm{vr}}}{q_3^2} \times \frac{\theta^2}{(1-\theta)^2}e^{-(2V_{\mathrm{a}}-E_{\mathrm{diss}})/k_{\mathrm{B}}T}e^{2\mu^{(\mathrm{lat})}/k_{\mathrm{B}}T}\,. \qquad (3)$$

Here $(2V_a - E_{\mathrm{diss}}) = -2V_0$ is, to within vibrational energies, the energy required to desorb two atoms from the substrate and associate them in the gas phase. Z_{vr} is the partition function accounting for the internal vibrations and the rotations of O_2 in the gas phase and $\mu^{(\mathrm{lat})}(\theta, T)$ is the contribution to the chemical potential of the adsorbate due to the lateral interactions in the Hamiltonian (1). With respect to obtaining the sticking coefficient, we note that initially dissociation is not activated, but at (local) coverages of $\theta \gtrsim 0.5$, O_2 dissociation is kinetically hindered by energy barriers [15, 21]. Under these circumstances, to obtain the coverage- and temperature-dependent sticking coefficient from first principles would represent a study of its own. In principle, this could be done following the approach described in the introduction for hydrogen dissociation. Instead we have used an expression that approximates the behavior that has been measured in the temperature regime of desorption [21], namely, $S_{\mathrm{dis}}(\theta) = S_0\exp\left[-(\theta/\sigma)^2\right]$, with $S_0 = 0.27$ and $\sigma = 0.3$: The sticking coefficient drops approximately as $(2/3-\theta)^2$ and for coverages above $2/3$ it remains very small up to a monolayer.

In Fig. 4 we show the calculated desorption rate [39] (left panel) of O_2 for various initial coverages as a function of substrate temperature. In the right panel, corresponding experimental results of Böttcher et al. [40] are shown. It can be seen that for low initial coverage the theory finds oxygen desorbs at about 100 K higher temperature than in experiment; this reflects an overbinding of the O atoms. We believe that this size of error is typical for present-day state-of-the-art DFT-GGA calculations. Aside from this, it can be seen that the theoretical spectra nicely reproduce the features of the experimental data, namely, a shift of the peak maxima to lower temperatures for higher initial coverages due to the repulsive interactions. The steepening of the leading edge for higher initial coverages as compared to coverages less than about 0.25 (where they are symmetric and rounded) is due to repulsive next-nearest-neighbor interactions and to a rapidly decreasing sticking coefficient which means that desorption is delayed to higher temperatures and the last third of a monolayer desorbs over a very narrow temperature range. We note that this effect has also been reported and discussed for oxygen at the silver surface [41]. In relation to the possibility of spillover as mentioned above, we tested whether omitting occupation of the fcc sites had an effect on the spectra; we found that for this system there was negligible change in the features. Neglecting the trio interactions, however, resulted in an increase of the overall repulsion and broadened the TPD spectra with desorption starting around 100 K lower; thus they play a rather important role for the higher coverages.

In Fig. 5 we show the isosteric heat of adsorption for a few temperatures: that is, the energy released when an O_2 molecule adsorbs dissociatively on the surface to yield the indicated coverage. At the highest temperature it shows a smooth decrease; at the lowest temperature, sharp peaks and dips occur at 1/4, 1/2, 3/4, and 1 ML. These coverages in fact correspond to the ordered phases that form in nature, i.e. the (2×2)-O [13] and (2×1)-O [14] phases for coverages 1/4 and 1/2 that were identified from early low-energy electron diffraction (LEED) intensity analyses with experiments performed under standard UHV conditions; the (2×2)-3O [16–18] and (1×1)-O [15] phases are more recent and had been predicted on the basis of DFT-GGA calculations; they require higher exposures of O_2 or the use of atomic oxygen obtained from, for example, highly oxidative species such as NO_2 for their formation. The rises in between

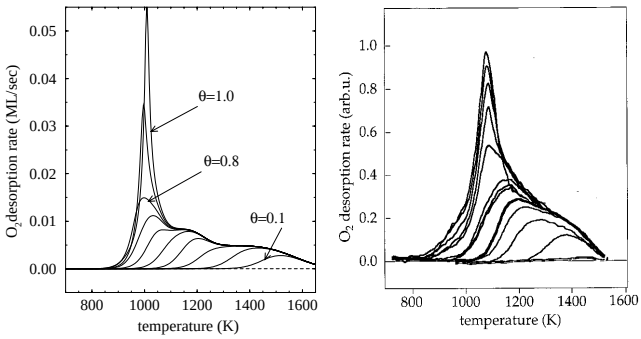

Fig. 4. Theoretical (*left panel*) and experimental (*right panel*) TPD spectra for associative desorption of O from Ru for a heating rate of 6 K/s. For the theoretical results, the initial coverages are $\Theta = 0.1$ to 1.0 in steps of 0.1; for the experimental results the initial coverage region also spans $\theta \to 0$ to 1 ML (from [40])

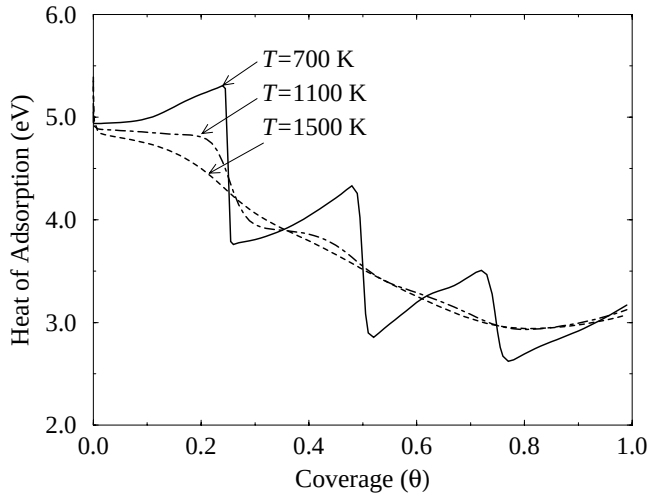

Fig. 5. The isosteric heat of adsorption of O_2 on Ru as a function of coverage for different temperatures

the dips in Fig. 5 originate from the attractive third-neighbor interactions, and also from the attractive trio interactions at higher coverages.

To summarize, we have described our first-principles-based approach that combines microscopic and macroscopic theories. This formalism was applied to the system of oxygen at a ruthenium surface. The good agreement with available experimental data thus confirms the efficacy of a predictive simulation of surface thermodynamics and kinetics. We mention that the theoretical approach described above can also be applied to more complex situations, for example, subsurface and multi-layer adsorption/desorption [12, 24].

2 Catalytic oxidation of CO

We turn now to our study of the oxidation of carbon monoxide. Clearly the gas phase reaction of $CO + 1/2O_2$ to form CO_2 is exothermic; it takes considerable energy however to break the O_2 bond. A good catalyst for this reaction therefore serves as a means to effectively dissociate the O_2 molecule but not to bind the O atoms too strongly and, importantly, to reduce the activation barrier to form the product, without partaking in the reaction itself and at best without forming toxic or volatile intermediatories that can also deplete the valuable catalyst material. With respect to the 'reactivity' of a surface, this usually refers to its ability to break bonds of an approaching molecule and to adsorb the fragments, which is often the rate limiting step in catalytic reactions.

The catalytic oxidation of CO has been studied intensively over the years (for example [42, 43]) due to its technological importance and its simple, prototypical nature, yet very little is actually known about the reaction path on a *microscopic* level. Recently, several first-principles studies have been reported which have shed some light in this direction. For example, in addition to our studies as briefly described below for reaction over the ruthenium surface, the studies of [44, 45] focused on reaction over the Pt(111) surface for the case of "low" oxygen coverages (0.25 ML). These studies revealed, among other things, that a favorable reaction pathway proceeds by CO diffusion towards a neighboring O atom. In the calculations, this causes a notable weakening of the O–metal bond strength (the main origin of the activation energy barrier), apparently due to competition for bonding charge of the metal atoms which results in the O atom (which is free to move since it has no close-by O neighbors) moving towards the less favorable bridge site (compared to the fcc site which is the energetically most favorable), thus enabling it to react with the CO molecule. The corresponding transition state was found to be a bent complex with the newly formed C−O bond lying almost parallel to the surface.

With respect to CO oxidation over the ruthenium surface, under usual UHV conditions (where the maximum attainable coverage of O is close to half a monolayer), co-adsorption of CO and O on Ru(0001) does not lead to any appreciable thermal activation to CO_2, in contrast to other transition metals [42, 43]. Very recently, however, it has been found that reaction can in fact be initiated under standard UHV conditions through irradiation by fs laser pulses [46]. Apparently, electronic excitations from the metal substrate into antibonding states in the region of the O−Ru bond substantially weaken it, thus enabling formation of CO_2. Also, studies performed with high partial gas phase pressures and oxidizing conditions (for example 16 Torr CO, 8 Torr O_2) and elevated temperatures (for example 300–500 K) using high-pressure catalytic reactors have, surprisingly, shown that the trend of low reactivity reverses and *highest* rates are found over the ruthenium surface [43, 47, 48] as compared to other transition metals. That is, this system appears to be a prime example of one which exhibits the so-called pressure-gap phenomenon. Additional studies indicate, that this reverse in reactivity can largely be related to the behavior of oxygen at ruthenium since under these reaction conditions, high oxygen surface concentrations of approximately 1 ML are present, whereas under UHV only a coverage of ≈ 0.5 ML can be achieved. This is possible since at high O_2 gas pressures there will be a high attempt frequency of impinging molecules to overcome activation barriers to dissociation. Interestingly here, negligible amounts of CO were detected during or after reaction. For the other metals (Pt, Pd, Rh, Ir), on the other hand, for highest rates of CO_2 production, the surface concentration of O was notably lower than 1 ML and that of CO easily detectable. Thus, for the same conditions it appears that in the competition for surface sites between CO and O, O wins on the ruthenium surface but CO wins on the other metal surfaces, which in fact can lead to poisoning of the reaction due to excess CO adsorption. The reason for the enhanced rate has thus been attributed to these high coverages of O [43] where the O−Ru bondstrength is also notably weaker [15, 29]. Interestingly, a reaction mechanism was speculated [47] that proceeds directly between a CO molecule from the gas phase with an adsorbed O atom. By "direct" we mean that CO does not form a chemical bond, or is in thermal equilibrium, with the surface prior to reaction; it may however physisorb or "bounce" across the surface before reacting [49]. These kind of reaction mechanisms have so far only been experimentally confirmed in a relatively small number of cases [50]; usually surface reactions proceed by both particles being chemisorbed on the surface, they diffuse around and then react to form the product (i.e., a so-called Langmuir–Hinshelwood reaction, see upper panel of Fig. 7).

Using DFT-GGA, we investigated the energetics of the interaction and reaction of CO with the O-covered Ru surface.

Details of this study have been reported in [51] so here we just briefly describe the results. We found that CO could not adsorb on the surface in the presence of the (1×1)-O structure, thus ruling out a L–H mechanism. We proceeded to investigate a direct scattering reaction. To do this, an appropriate cut through the high-dimensional PES was constructed, namely, one involving the position of the C atom of CO above the surface and the position of the reacting O(a) atom below it. At each point of the PES (constructed by about 100 ab initio points) all the atoms were fully relaxed (except the O(a) and C atoms being held fixed and the bottom two Ru layers). The minimum energy pathway was found to correspond to a transition state with a bent configuration; namely, one with a bond angle of $\approx 131°$ and C−O bond lengths of 1.17 Å and 1.50 Å (the new C−O(a) bond) with an associated activation barrier of about 1.1 eV. The origin of the barrier was found to be due to Pauli repulsion between the negatively charged O adatom and the occupied CO 5σ orbital [51]. Once the energy barrier is overcome and the CO_2 molecular bond is formed, the bond axis straightens out and the product is strongly repelled from the surface towards the gas phase.

Using a simple Arrhenius equation with the obtained activation energy barrier, an estimate for the reaction rate was made, taking the prefactor ($7.5 \times 10^6\ s^{-1}$) to be the frequency of impinging CO molecules per surface Ru atom for a given CO pressure (16 Torr) and temperature (500 K). The rate was found to be far lower than experiment (by 3×10^{-6}) which indicates that direct scattering is not the dominant mechanism but that it may occur with a low probability. We recognise that this simple estimate is rather crude and assumes that the reaction proceeds along a one-dimensional reaction coordinate and that there is one well-defined transition state. For chemical reactions at surfaces this concept can be misleading since the dimension of phase-space is so high that not just one, but many transition states exist, and all of them may play a role. Nevertheless, for several approaches of CO from the gas phase towards the O adatom, this barier was the lowest found so that we may expect that our estimate represents an *upper* bound for the reaction rate via this mechanism.

Another possibility is that CO might adsorb at O vacancies. [Because the surface is in contact with high partial pressures of CO and O_2, due to the law of mass action, there will be a concentration of mixed O and CO on the surface as determined by the thermodynamics (for example relative adsorption energies of CO and O) and the kinetics [51]]. With respect to determining a low-energy reaction pathway, we note that this is a very complex problem since the positions of CO and the reacting O atoms have to be considered, as well as relaxations of neighboring O atoms and the substrate. As a first step we investigated the adsorption of CO into the O vacancy; interestingly, it was found to be activated, i.e., there is a small energy barrier of about 0.3 eV. On overcoming the barrier, which should be readily possible at the high pressures employed, the adsorption energy of CO relative to free CO in vacuum, is about 0.85 eV. (Compare to the stronger binding of the O atom at this coverage, i.e., 2.15 eV (or about 5.13 eV with respect to a free O atom)). With respect to the reaction pathway, initially we kept the lateral positions of the atoms fixed for a given configuration of the reactants, but allowed vertical atomic relaxations. In this way we tested many possible reaction paths. We found that the lowest energy reaction pathway was for CO to diffuse and approach an adsorbed O adatom. The transition state of the reacting complex was found to have a bond angle of about 125° and C−O bond lengths of 1.18 Å and 1.59 Å (the new C−O(a) bond); rather similar to the transition state for the scattering reaction described above. On the other side of the energy barrier the forces become attractive, the complex straightens out its bond and becomes linear, and the CO_2 molecule leaves the surface. The activation energy barrier that corresponds to the transition state is about 1.5 eV, and there is an energy gain on CO_2 formation of about 0.66 eV (see Fig. 6). We point out that allowing lateral relaxations of neighboring atoms may lead to a lower barrier and and even other low energy pathways; this will be investigated in future work. In Fig. 7 (lower panel) we show the valence electron density for some selected positions along the reaction path where the weakening of the CO– and O–metal bonds can be noticed as CO nears the adsorbed O atom, as well as the formation of the new C–O(a) bond.

We note that the energy barrier is larger than that of the direct scattering reaction, but here, the effective prefactor in an Arrhenius equation will be much larger also since the reactants are adsorbed on the surface (for example 10^{13} is often assumed for particles chemisorbed on surfaces; this value, however, can vary widely depending on the system). In [44, 45] for the study of CO oxidation over Pt(111), the minimum energy pathway was determined by employing various algorithms (for example in [45] a so-called nudged elastic band method was used). We used however the standard grid approach of calculating many points in the PES, since we are also interested in the *shape* of the PES away from a one-dimensional low-energy pathway for use in future work.

Interestingly, recently it has been found that after completion of the monolayer structure of oxygen on Ru(0001), high concentrations of atomic oxygen can enter the surface region [29, 40, 52, 53] for very high O_2 exposures (or with the use of NO_2) at elevated temperatures (for example $\gtrsim 600$ K). For concentrations greater than 3 ML, the rate of CO_2 formation in this temperature range has been reported to be two orders of magnitude higher than that when there is only on-surface oxygen present [40]. Furthermore, for a surface with very high concentrations of O, when it is cooled to room temperature (which prevents significant movement of the O atoms) it has been found that additional O and CO can adsorb

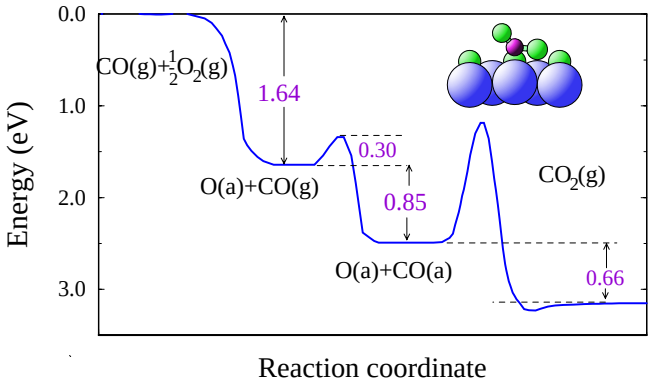

Fig. 6. Calculated energy diagram for the Langmuir–Hinshelwood mechanism of CO oxidation at Ru(0001). The *inset* shows the corresponding transition state where the *large*, *small*, and *small dark circles* represent Ru, O, and C atoms, respectively

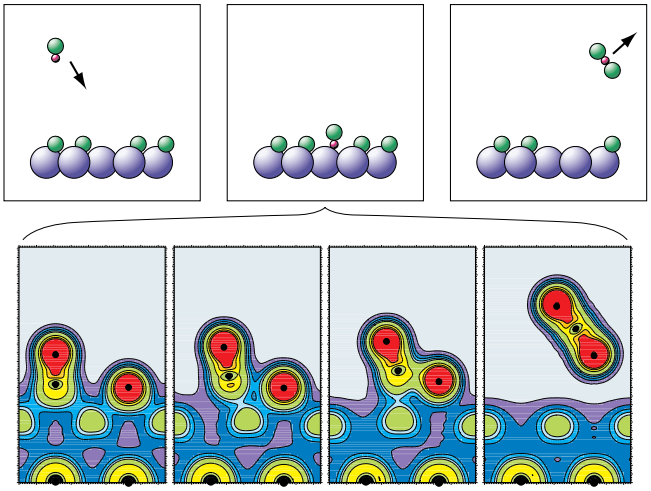

Fig. 7. Schematic illustration of the Langmuir–Hinshelwood process (*upper panels*) and the valence electron density distribution for selected positions along a low energy reaction path (*lower panels*). The first contour line corresponds to 2×10^{-2} and the contour spacing is 2×10^{-2} for the first five contour lines, thereafter the spacing is 1×10^{-1}. The units are given in e bohr^{-3}

on the O-covered surface, and CO_2 formation proceeds with an even higher rate [54, 55]. The exact microscopic mechanisms by which the reaction rate is enhanced is at present unclear, as is the precise location and bonding nature of the additional (for example, subsurface) O atoms.

We note that despite its high reactivity for CO oxidation, Ru will not be used in automotive catalysts because volatile Ru oxides are formed under operating conditions. Nevertheless, trying to understand why Ru is so much more effective than other transition metals may help in the design of materials with similar properties. Furthermore, there is an interesting and likely conceptionally important aspect of Ru studies: Ru can exist in many oxidation states with the result that its surface region can be loaded with high concentrations of oxygen. This poses the question of whether it is appropriate to call the reactive surface an adsorbate system, or if it is more appropriate to call it a type of "surface oxide" (for example, a RuO_2-like system in the present case).

3 Subsurface oxygen at $(1 \times 1) - \mathbf{O}/\mathbf{Ru}(0001)$

As described above, after completion of an oxygen monolayer on Ru(0001), high uptakes of atomic oxygen into the surface can occur at elevated temperatures and with very high O_2 exposures (or with the use of atomic oxygen via a highly oxidative species, for example NO_2). The chemical properties and adsorption sites of the additional O atoms are unknown at present. Recent experiments indicate that these oxygen species are responsible for high CO_2 formation rates, probably by serving as a reservoir of atomic oxygen [40, 53, 54] that become available reaction partners at high temperatures; they could also conceivably act to modify the chemical bond of the on-surface O atoms making them more reactive, or they could serve to significantly alter the electronic properties of the surface so that additional O and CO can adsorb on the surface thus opening up another possible reaction channel for CO_2 formation; indeed the latter is indicated in the studies of [54, 55].

At other transition-metal surfaces, oxygen readily enters the subsurface region at notably lower temperatures and coverages than on ruthenium, where oxide formation can occur [56]. Oxide formation can have a detrimental effect with respect to the catalytic activity of a surface, for example, for the CO oxidation reaction [43]. For example, at 400 K the O/Pd(110) system already apparently shows formation of a surface oxide layer [57]. For O at Pt(111), where ozone (O_3) has been used as a source of atomic oxygen, experiments performed at 300 K (i.e. relatively low temperature) have found that a full monolayer is stable on the surface but is unstable at higher temperatures. For higher coverages (still at 300 K) it is reported that PtO_x particles nucleate, and at 2.4 ML an oxidic film forms [58]. Similarly, at the Rh(111) surface, with the use of *atomic* oxygen (i.e. here the constraint of using a molecular oxidant was lifted by creating a beam of "real" O atoms from dissociated O_2) an ordered (1×1)-O phase forms just as on Ru; here, however, the adlayer is only stable to 400 K, beyond which oxygen apparently "dissolves" into the bulk [59, 60]. On Ru, the (1×1) phase does not convert to subsurface sites, but is stable to higher temperatures and only desorbs from the surface with increasing temperature. For the O/Rh(111) system, the adsorption site of a subsurface oxygen species has recently been determined by X-ray photoelectron diffraction [61, 62]. The subsurface species is found to occupy an octahedral site below the first metal layer; interestingly, occupation of this site is found to induce a site switch of the neighboring on-surface O atoms from fcc to hcp sites.

We have performed DFT-GGA calculations for various structures involving subsurface oxygen at Ru(0001). The details of the calculations are as described in [29]. Below we briefly summarize some of our results which will be presented in more detail elsewhere.

For all geometries investigated, we kept the (1×1)-O structure on the surface as is consistent with experiment and with our earlier theoretical investigations [51]. In the subsurface region between the top two Ru layers there are three possible sites: the octahedral site where O has six nearest-neighbor Ru atoms, three above and three below; and two tetrahedral sites where O has four nearest-neighbor Ru atoms; in the first site (t1), there are three Ru atoms above O and one below, and in the second (t2), the situation is just the opposite. We performed calculations for these different sites for two coverages of O below the first Ru layer, namely 1/4 and 1 ML; these correspond to *total* O "coverages" of 1.25 and 2 ML, respectively. In the following we discuss *average* adsorption energies per O atom, as given by (2), so that it should be kept in mind that also the effect of the on-surface O atoms is included and the O adsorption sites of the system do not have to be the same. We found the t2 site to be energetically the most favorable for 1/4 ML under the surface i.e. its average adsorption energy is 0.112 eV and 0.365 eV (or 0.560 eV and 1.825 eV per (2×2) cell with five O atoms per cell) greater than that of the octahedral and t1 sites, respectively, while for 1 ML, the octahedral site is preferred by 0.015 eV and 0.095 eV (or 0.150 eV and 0.950 eV per (2×2) cell with ten O atoms per cell) with respect to the t2 and t1 sites. To date there has been no experimental determination of subsurface adsorption sites with which we can compare.

We find that the atomic relaxations induced by the presence of subsurface oxygen are significant and it is therefore not accurate to assume that the Ru lattice will remain essentially undisturbed by occupation of subsurface sites. For example, for 1 ML under the surface the octahedral, t1, and t2 sites induce an expansion of the first metal interlayer spacing of 1.21 Å, 1.50 Å, and 1.38 Å, respectively. A similar-sized (local) displacement was reported for O under the first Rh(111) layer [61, 62]. It is interesting to note that for O in the octahedral site at 1 ML coverage (2 ML total coverage), each surface Ru atom has six nearest-neighbor O atoms, three above and three below. In ruthenium dioxide, RuO_2, which belongs to the family of transition metal dioxide compounds with rutile-type structure (D_{4h} symmetry), the Ru atoms are also surrounded by a nearly octahedral array of six oxygen ions.

Another consideration is whether it is energetically favorable for O to stay under the first Ru layer or to reside deeper in the bulk. We tested this by placing O atoms (in octahedral sites) between the second and third Ru layers for coverages of 1/4 and 1 ML. In both cases this position is energetically *less* favorable than for the sites directly under the top Ru layer. Thus there is a preference for O atoms to be closer to the surface and to other O atoms (or to other O−Ru bonds) rather than being isolated in the bulk.

To investigate the interaction between the subsurface O atoms, we considered two additional structures, namely those with 0.5 and 0.75 ML below the surface (1.5 and 1.75 ML total coverages). Here we placed the O atoms in the octahedral sites. We find that for coverages of 0.5 to 1 ML below the first layer, the average adsorption energy of the system *increases*, i.e., becomes more energetically favorable with increasing coverage (see the dot-dashed line in Fig. 8). This indicates an *attractive* interaction between the subsurface O atoms which implies that there may be a tendency to form subsurface "islands". We note that indication of this behavior was also reported in an early theoretical study of O at Ni(001) [63]. In this work the origin was explained in terms of the energy cost of distorting the substrate lattice: to place the first O atom in a subsurface site the crystal lattice significantly distorts to accommodate it and there is a high energy cost; on addition of a second atom in the subsurface region, since the substrate atoms are already displaced in the neighborhood of the first O atom, it is energetically favorable for the second atom to adsorb nearby, rather than as an isolated particle that must again create a significant displacement of substrate atoms. Similarly for the addition of subsequent atoms in the subsurface region. In Fig. 8 we show the calculated average adsorption energy as a function of coverage. We also include the coverage region from $\Theta = 1/9$ to 1 where O occupies on-surface hcp sites, as well as higher total coverages of O; namely, we also performed calculations for 3 ML and 4 ML (total coverage), where again O is placed in the octahedral sites. In Fig. 8 we join the calculated values for 1, 2, 3, and 4 ML to guide the eye but note that we expect a similar behavior as occurs between 1 and 2 ML for the coverage region between 2–3 ML and 3–4 ML if we would similarly consider fractional monolayer coverages below the surface, filling first the available octahedral sites closest to the surface. It can be clearly seen that the adsorption energy of O in the subsurface region is notably *weaker* compared to on-surface oxygen ($\Theta \leq 1$ ML), but that with respect to the energy of $1/2O_2$ (≈ 3 eV), the adsorption is still appreciably exothermic at all coverages investigated. Oxygen therefore will prefer to stay on the surface and only when there are no on-surface sites available, and only if kinetic barriers can be overcome, will O occupy subsurface sites. This is consistent with the picture of [40, 53–55] where the Ru surface can be loaded with high concentrations of a weakly bound O species (as attributed to giving rise to the enhanced CO_2 formation rate).

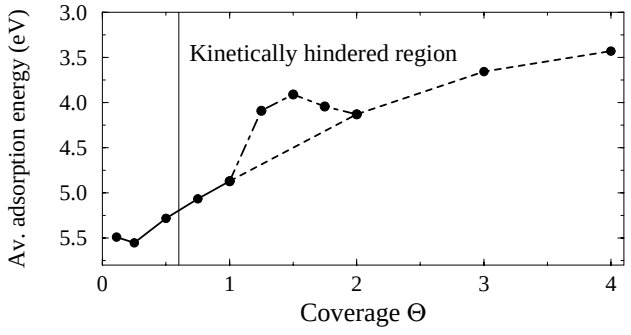

Fig. 8. Average adsorption energy of O on Ru(0001) as a function of coverage. For on-surface adsorption, O occupies hcp sites (i.e. up to one monolayer) and additional O atoms are placed in octahedral subsurface sites. The region not accessible to standard UHV experiments is indicated and lies to the right of the *vertical line*

Finally, to learn the effect of subsurface oxygen on the bonding of on-surface O to Ru, we calculate the energy cost to remove one of the on-surface O atoms of the (1×1) monolayer structure and to put it into an O_2 dimer in the gas phase. We do this for different amounts of oxygen immediately under the surface (for O in the octahedral site) and compare the result to the case of no subsurface oxygen: In particular, we consider 1/4, 1, and 2 ML of subsurface O (i.e. total O coverages of 1.25, 2, and 3 ML, respectively). Alternatively, this energy cost can be thought of as the energy an O atom from an O_2 dimer in the gas phase gains on adsorbing onto the vacant hcp site. We find that in contrast to a reduction in the on-surface O−Ru bond strength, as may be expected from the understanding of competitive adsorption of electronegative species, subsurface O *stabilizes* the on-surface O−Ru bond, namely by 1.08 eV [64], 0.57 eV, 0.51 eV, for the respective subsurface O coverages considered. Since the on-surface O−Ru bond is not weakened by the presence of subsurface O but strengthened, this suggests that on-surface O will not be more reactive towards CO and CO_2 formation, but rather the more weakly bound subsurface O species plays the active role under these reaction conditions; it is also possible as mentioned above that the presence of the additional "subsurface" O species alters the electronic structure of the surface as a whole, allowing it to support additional adsorbed O atoms (and CO) on the O-covered surface. This will be investigated in future work.

References

1. See for example, H. Topsoe, M. Boudart, J.K. Nørskov (Eds.): ''Frontiers in catalysis: Ammonia synthesis and beyond". Topics in Catal. **1**, 185 (1994)
2. A. Gross, M. Scheffler: Phys. Rev. B **57**, 2493 (1998)

3. A. Gross: Surf. Sci. Rep. **32**, 291 (1998)
4. G.J. Kroes, E.J. Baerends, R.C. Mowrey: Phys. Rev. Lett. **81**, 4781 (1998)
5. B. Hammer, K.W. Jacobsen, J.K. Norskov: Phys. Rev. Lett. **70**, 3971 (1993)
6. B. Hammer, M. Scheffler, K.W. Jacobsen, J.K. Norskov: Phys. Rev. Lett. **73**, 1400 (1994)
7. M. Born, R. Oppenheimer: Ann. Phys. Lpz. **84**, 457 (1927)
8. P. Ruggerone, C. Ratsch, M. Scheffler: In *Growth and Properties of Ultrathin Epitaxial Layers*, ed.by D.A. King, D.P Woodruff, The Chemical Physics of Solid Surfaces, Vol. 8. (Elsevier, Amsterdam 1997), p. 490
9. P. Kratzer, M. Scheffler: to be published.
10. N. Moll, M. Scheffler, E. Pehlke: PHys. Rev. B **58**, 4566 (1998)
11. A. Zunger: In *Statics and Dynamics of Alloy Phase Transformations*, Eds. P.E.A. Turchi, A. Gonis, NATO ASI Series (Plenum Press, New York 1994) p.361
12. H.J. Kreuzer, S.H. Payne: In *Computational Methods in Surface Science and Colloid Science*, ed. by M. Borowko, Marcel Dekker (1999)
13. H. Pfnür, D. Held, M. Lindroos, D. Menzel: Surf. Sci. **220**, 43 (1989)
14. M. Lindroos, H. Pfnür, D. Held, D. Menzel: Surf. Sci. **222**, 451 (1989)
15. C. Stampfl, S. Schwegmann, H. Over, M. Scheffler, G. Ertl: Phys. Rev. Lett. **77**, 3371 (1996)
16. K.L. Kostov, M. Gsell, P. Jakob, T. Moritz, W. Widdra, D. Menzel: Surf. Sci. **394**, L138 (1997)
17. Y.D. Kim, S. Wendt, S. Schwegmann, H. Over, G. Ertl: Surf. Sci. **418**, 267 (1998)
18. M. Gsell, M. Stichler, P. Jakob, D. Menzel: Israel J. Chem. **38**, 339 (1999)
19. P. Piercy, K. De'Bell, H. Pfnür: Phys. Rev. B **45**, 1869 (1992)
20. T.E. Madey, H.A. Engelhardt, D. Menzel: Surf. Sci. **48**, 304 (1975)
21. L. Surnev, G. Rangelov, G. Bliznakov: Surf. Sci. **159**, 299 (1985)
22. C. Stampfl, H.J. Kreuzer, S.H. Payne, H. Pfnür, M. Scheffler: Phys. Rev. Lett. **83** (1999)
23. H.J. Kreuzer, S.H. Payne: In *Equilibria and Dynamics of Gas Adsorption on Heterogeneous Solid Surfaces*, ed. by W. Rudziński, W.A. Steele, G. Zgrablich, Vol. 104 (Elsevier, Amsterdam 1997) p. 153
24. S.H. Payne, H.J. Kreuzer: Surf. Sci. **399**, 135 (1998)
25. N. Troullier, J.L. Martins: Phys. Rev. B **43**, 1991 (1993)
26. M. Fuchs, M. Scheffler: Comput. Phys. Commun. **116**, 1 (1999); http://www.fhi-berlin.mpg.de/th/fhimd.html
27. R. Stumpf, M. Scheffler: Comput. Phys. Commun. **79**, 447 (1994); M. Bockstedte, A. Kley, J. Neugebauer, M. Scheffler: Comput. Phys. Commun. **107**, 187 (1997); http://www.fhi-berlin.mpg.de/th/fhimd.html
28. J.P. Perdew, J.A. Chevary, S.H. Vosko, K.A. Jackson, M.R. Pederson, D.J. Singh, C. Fiolhais: Phys. Rev. B **46**, 6671 (1992)
29. C. Stampfl, M. Scheffler: Phys. Rev. B **54**, 2868 (1996); Surf. Sci. **377-379**, 808 (1997)
30. S. Renisch, R. Schuster, J. Wintterlin, G. Ertl: Phys. Rev. Lett. **82**, 3839 (1999)
31. J. Wintterlin, J. Trost, S. Renisch, R. Schuster, T. Zambelli, G. Ertl: Surf. Sci. **394**, 159 (1997)
32. T.S. Rahman, A.B. Anton, N.R. Avery, W.H. Weinberg: Phys. Rev. Lett. **51**, 1979 (1983)
33. B.G. Johnson, P.M.W. Gill, J.A. Pople: J. Chem. Phys. **98**, 5612 (1993)
34. C. Domb: Adv. Phys. **9**, 149 (1960)
35. P.A. Rikvold, W. Kinzel, J.D. Gunton, K. Kaski: Phys. Rev. B **28**, 2686 (1983)
36. N.C. Bartelt, T.L. Einstein, L.D. Roelofs: Phys. Rev. B **34**, 1616 (1986)
37. W. Kinzel, M. Schick: Phys. Rev. B **23**, 3435 (1981)
38. N.H. Fuchs: Phys. Rev. B **41**, 2173 (1990)
39. Calculations performed with the ASTEK package written by H.J. Kreuzer, S.H. Payne (available from Helix Science Applications, 618 Ketch Harbour Road, Portuguese Cove, N.S. B3V1K1, Canada)
40. A. Böttcher, H. Niehus, S. Schwegmann, H. Over, G. Ertl: J. Phys. Chem. **101**, 11 185 (1997)
41. F. Buatier de Mongeot, M. Rocca, A. Cupolillo, U. Valbusa, H.J. Kreuzer, S.H. Payne: J. Chem. Phys. **106**, 711 (1997)
42. T. Engel, G. Ertl: J. Chem. Phys. **69** (1978) 1267; Adv. Catal. **28**, 1 (1979); *The Chemical Physics of Solid Surfaces and Heterogeneous Catalysis*, ed. by D.A. King, D.P. Woodruff, Vol. 4 (Elsevier, Amsterdam 1982)
43. C.H.F. Peden: In *Surface Science of Catalysis: In situ Probes and Reaction Kinetics*, ed. by D.J. Dwyer, F.M. Hoffmann (Am. Chem. Soc., Washington, DC 1992)
44. A. Alavi, P. Hu, T. Deutsch, P.L. Silvestrelli, J. Hutter: Phys. Rev. Lett. **80**, 3650 (1998)
45. A. Eichler, J. Hafner: Phys. Rev. B **59**, 5960 (1999)
46. M. Bonn, S. Funk, C. Hess, D.N. Denzler, C. Stampfl, M. Scheffler, M. Wolf, G. Ertl: Science **285**, 1042 (1999)
47. C.H.F. Peden, D.W. Goodman, M.D. Weisel, F.M. Hoffmann: Surf. Sci. **253**, 44 (1991)
48. C.H.F. Peden, D.W. Goodman: J. Phys. Chem. **90**, 1360 (1986)
49. J. Harris, B. Kasemo: Surf. Sci **105**, L281 (1981)
50. E.W. Kuipers, A. Vardi, A. Danon, A. Amirav: Phys. Rev. Lett. **66**, 116 (1991); C.T. Rettner: Phys. Rev. Lett. **69**, 383 (1992); C.T. Rettner, D.J. Auerbach: Phys. Rev. Lett. **74**, 4551 (1995); C.T. Rettner: J. Chem. Phys. **101**, 1529 (1994)
51. C. Stampfl, M. Scheffler: Phys. Rev. Lett. **78**, 1500 (1997); J. Vac. Sci. Technol. A **15**, 1635 (1997); Surf. Sci. **377-379**, 808 (1997); Surf. Sci. **433–435**, 119 (1999)
52. W.J. Mitchell, W.H. Weinberg: J. Chem. Phys. **104**, 9127 (1996)
53. A. Böttcher, H. Niehus: J. Chem. Phys. **110**, 3186 (1999)
54. A. Böttcher, H. Niehus: submitted to Phys. Rev. B
55. A. Böttcher, M. Rogozia, H. Niehus, H. Over, G. Ertl: J. Phys. Chem. B **103**, 6267 (1999)
56. D.G. Castner, G.A. Somorjai: Appl. Surf. Sci. **6**, 29 (1980)
57. V.A. Bondzie, P. Kleban, D.J. Dwyer: Surf. Sci. **347**, 319 (1996)
58. N.A. Saliba, Y.-L. Tsai, C. Panja, B.E. Koel: Surf. Sci. **419**, 79 (1999)
59. K.D. Gibson, M. Viste, E.C. Sanchez, S.J. Sibener: J. Chem. Phys. **110**, 2757 (1999)
60. K.A. Peterlinz, S.J. Siebener: J. Phys. Chem. **99**, 2817 (1995)
61. J. Wider, T. Greber, E. Wetli, T.J. Kreutz, P. Schwaller, J. Osterwalder: Surf. Sci. **417**, 301 (1998)
62. T. Greber, J. Wider, E. Wetli, J. Osterwalder: Phys. Rev. Lett. **81**, 1654 (1998)
63. B. Chakraborty, S. Holloway, J.K. Nørskov: Surf. Sci. **152-153**, 660 (1985)
64. The value of 1.08 eV corresponds to removing (or adding) one of the three on-surface O atoms, in the hcp sites of the (2×2) surface cell, which binds to two Ru atoms that also share bonds with the subsurface O atom – as opposed to the alternate on-surface hcp O atom that binds to only one Ru atom that shares a bond with the subsurface O atom